Experimental Studies of the Turbulent Wake behind Self-Propelled Slender Bodies

J. A. Schetz* and A. K. Jakubowski†
Virginia Polytechnic Institute and State University, Blacksburg, Va.

The turbulent wakes behind a drag body, a jet-propelled body, and a propeller-driven body all with the same streamlined forebody shape were studied experimentally in a subsonic wind tunnel at a nominal Reynolds number based on diameter of 6×10^5. The wakes produced by the latter two bodies were momentumless. Mean flow and turbulence data were taken at five axial stations ($X/D=2$, 5, 10, 20, and 40) downstream of the sterns of these bodies. The data for the wake behind the drag body compare favorably with previous experiments and establish a rigid reference for the wakes behind the self-propelled configurations. The downstream rate of decay of the velocity defect is essentially the same for the drag and propeller-driven bodies, whereas the decay for the jet-propelled body is substantially faster. The magnitude of the axial turbulence intensity is greater for the jet-propelled model than the other models, and the absolute value of the radial shear stress is greater (beyond $X/D=2$) for the propeller-driven model. The rate of decay of the axial turbulence intensity is faster for the propeller-driven model than the jet-propelled model, however the rate of decrease of radial shear stress is faster for the jet propelled model.

Nomenclature

C_D	= body drag coefficient
C_T	= propeller thrust coefficient
D	= maximum diameter of model
J	= propeller advance ratio
n	= revolutions per sec
P	= pressure
q	= dynamic pressure
Re	= Reynolds number
R	= maximum radius of models
T	= thrust
u,v_r,v_t	= mean velocity components in the x, r, θ directions
u',v',w'	= turbulent velocity components in the x, r, θ directions
$(u'^2)^{1/2}$	= axial turbulence intensity
$-\overline{u'v'}$	= radial Reynolds shear stress
$-\overline{u'w'}$	= tangential Reynolds shear stress
U	= mean total velocity
x,r,θ	= axial, radial, and tangential coordinates
η_p	= propeller efficiency
ρ	= density
Subscripts	
c	= center of wake
e	= edge of wake

Introduction

THE great bulk of experimental information on turbulent shear flows behind bodies moving in a fluid is restricted to the unpropelled or "drag-body" situation. This is, perhaps, surprising, since most practical devices are self-propelled, but it is nonetheless true. Indeed, in recent times, virtually all estimates of the development of wakes behind self-propelled bodies have been based on the basic experiment of Naudascher[1] even though the configuration employed was not representative of any body of engineering interest. A tabular presentation of the primary experimental cases available for turbulent wakes behind bodies in low speed flow, unpropelled and self-propelled, is included in Table 1.

This experimental program was conceived to provide a systematic comparison of the turbulent wakes behind slender bodies with identical forebody shape by varying through the following cases: 1) pure drag body, 2) self-propelled by axial fluid injection, 3) self-propelled with a well designed propeller. Here "well designed" is taken to mean matched to the nominal operating conditions of the experiment. Tests were done in a large (6 ft × 6ft) subsonic wind tunnel at a high speed (206 fps), so that a Reynolds number based on diameter of nominally 6.18×10^5 could be achieved. This is more than an order of magnitude larger than previous propeller-driven laboratory tests.[14] For each model, mean flow stagnation and static pressure profile measurements were made with a pitot-static tube at five axial stations: $X/D=2$, 5, 10, 20, and 40. Flow angularity was determined with a wedge-type directional probe, and a Kiel probe was employed to measure total pressure when required. The following turbulence intensity and Reynolds shear stress values were obtained using straight and slanted hot wires, respectively: $(\overline{u'^2})^{1/2}$, $(\overline{v'^2})^{1/2}$, $(\overline{w'^2})^{1/2}$, $\overline{u'v'}$, and $\overline{u'w'}$. Complete details and tabulated data are available in Refs. 15 and 16. In this paper, only mean-flow velocity, axial turbulence intensity, and radial shear stress profiles are given due to space limitations.

Facilities and Models

Wind Tunnel

Tests were conducted in the VPI & SU Low-Speed Wind Tunnel where the main test section is 6 ft × 6 ft and 23 ft long. These experiments were all run at the tunnel dynamic pressure q of 9.5 in. H_2O, which corresponds to a nominal speed of 206 fps. The turbulence intensity of the tunnel air stream was about 0.1%.

Wind Tunnel Models

There were three models; all had a maximum diameter of 6.0 in. and were nominally 6.0 ft long. They were supported on the centerline of the tunnel by a thin (0.5 in.) strut that extended from the top of the tunnel. Each had a parabolic nose, a 3 ft cylindrical middle body, and a pointed stern.

Drag Body Model

A drawing of the drag body, which was called Model 1, is

Submitted, January 20, 1975; revision received May 14, 1975. This work was supported by the Office of Naval Research.

Index categories: Jets, Wakes, and Viscid-Inviscid Flow Interactions.

*Professor and Department Head, Aerospace and Ocean Engineering Department. Associate Fellow AIAA.

†Associate Professor, Aerospace and Ocean Engineering Department. Member AIAA.

Table 1 Low speed, axisymmetric turbulent wake experiments

Author	Year	Ref. No.	Momentumless	Mean Flow	Properties	Configuration
Hall and Hislop	1938	2		x		2:1 cylinder
Cooper and Lutzky	1955	3		x	x	Thin disks
Ilizarova and Pochkina	1962	4		x		6.67:1 body of revolution
Ridjanovic	1963	5	x	x	x	Circular disk with center jet
Carmody	1964	6		x	x	Circular disk with center jet
Wang	1965	7	x	x	x	Circular disk with center jet
Naudascher	1965	1	x	x	x	Circular disk with center jet
Ginevskii, Pochkina, and Ukhanova	1966	8	x	x	x	Circular disk with center jet
Buchinskaya and Pochkina	1966	9		x		6:1 Ellipsoid
Chevray	1968	10		x	x	6:1 Spheriod
Bukreev, Kostomakha, and Lytkin	1972	11		x	x	Slender body (8:1 prolongation)
Hokenson and Schetz	1973	12		x	x	Sphere
Bukreev, Kostomakha, and Lytkin	1974	13		x	x	Sphere and slender body
Gran	1974	14	x	x	x	Rankine Ovoid with Propeller
Swanson, Chieng, Schetz and Jakubowski	1974	15,16	x	x	x	Slender bodies with peripheral jet or propeller

shown in Fig. 1. The nose and stern parts of the model were constructed of wood, and the center section was made of aluminum tubing.

Jet-Propelled Model

The model that employed air injection propulsion, referred to as Model 2, had a Plexiglass nose, an aluminum middle section, and a stern formed by a slender, Plexiglass, tear-drop shaped center body held in position by four vanes spaced 90^0 apart. Air was injected through a 1-in. peripheral slot at the end of the parallel middle body. A drawing of the model is shown in Fig. 2. The air for injection was supplied by 150 psi compressors, and in this case, the strut was comprised of 17 parallel 0.25 in. diam tubes and two 0.5-in. diam pipes, one at the leading edge and the other at the trailing edge, for air passage into the model. It was given a smooth surface and airfoil shape the same as the solid strut used for the other bodies by covering it with polyester auto body filler.

The plenum chamber in the model was vented through a series of 0.313-in.-diam peripheral holes spaced 1.0 in. apart, and the air leaving these holes went through a series of coarse and fine screens. These screens served the dual purpose of flow straighteners and turbulence reducers.

Propeller-Driven Model

The propeller-driven model, designated Model 3, was simply the drag body model (Model 1) fitted internally with a 0.5 HP, 10,000 rpm a.c./d.c. motor operated d.c., overloaded to 12,200 rpm and a shaft, and externally with a propeller at the stern.

The propeller was a 6.0-in.-diam, three-bladed, plastic model airplane propeller. The blades were heated at the root and twisted with a special jig to yield a higher pitch (originally 3.0 in.) in order to operate efficiently at the high air speed of the tests. Propellers with a variety of pitches were tested in order to find the appropriate propeller to produce sufficient thrust to match the drag of Model 3. Complete details concerning the testing of the propellers and the results obtained are given in Ref. 15. In each case performance was analyzed by the change of both thrust coefficient C_T and efficiency η_p with advance ratio J. After considerable testing a propeller with a forward speed-to-rotational-speed ratio of 2.46, defined as the experimental mean diameter pitch, and an "open-water" efficiency of 68% was selected. The size of the propeller was scaled with respect to the size of the wake and not the size of the body. This scaling was accomplished by scaling wake diameter on the basis of Reynolds number, taking a "full-scale" case of a typical submarine.

Instrumentation

Pressure Measurements

The mean flow data were obtained with the following probes: 1) pitot-static tube, 2) yaw-head tube, and 3) Kiel probe. Pitot and static pressure measurements were made with a 0.0625-in.-diam straight pitot-static probe with static ports located 0.375 in. from the tip. A wedge-type flow direction sensor was used to find the flow yaw angle variation for the propeller-driven model. Finally, to insure the best possible accuracy for the measurement of total head when the flow in the wake was skewed with respect to the freestream direction, a Kiel probe with a 0.25-in.-diam Venturi sensing head and a 0.125-in.-diam probe was used. The pressures were measured on either a differential pressure transducer (range of 0-10 in. of H_2O) and/or an adjustable-angle multiple manometer, depending upon the number of readings required simultaneously. All pressure transducer signals were displayed on an integrating microvoltmeter and/or strip chart recorders. The d.c. digital voltmeter was equipped with a variable sample rate and a four-figure readout. An electronic

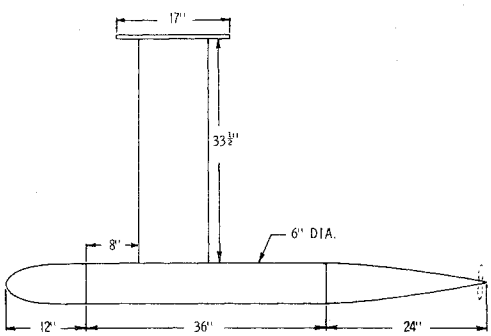

Fig. 1 Drag-body model.

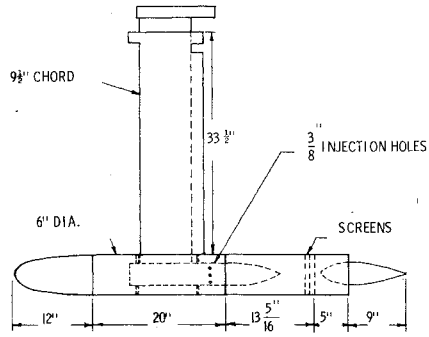

Fig. 2 Jet-propelled model.

manometer with digital readout was used to monitor the tunnel dynamic pressure.

Hot Wire Measurements

The turbulence data were obtained with a straight wire and 45^0 slant wire, hot-wire probes. Both had platinum plated, tungsten wires 0.00015 in. in diam. The cold resistance of the wires was 5-7 ohms, and they were operated at a 50% overheat. The signals were processed through a constant temperature anemometer (Model 1050 Thermo Systems) and were read on an rms digital voltmeter. Linearization of the output of the anemometer was not necessary because of the relatively low amplitude signals for the flowfields investigated. The rms voltmeter has a signal response range of 1 Hz to 400 KHz, integrator time constants from 0.1 to 30 sec, and an accuracy of 0.5% of the full-scale deflection. The straight wire probe was rotated 180^0 in each of two mutually orthogonal planes in order to obtain the three-component turbulent intensities and Reynolds stresses. This was accomplished automatically with a specially constructed apparatus.

Traversing Probe Mount

All probes were traversed through the wake at various axial stations by an automatic traversing mount. This traverse was approximately 50.5 in. high and had a vertical translation movement of 4 ft. The horizontal range was 5.5 in. to either side of the center point. Vertical and horizontal motion was controlled with variable-speed motors.

Calibration Procedure

The hot-wire probes and the yaw head probe were calibrated several times during each series of measurements. The velocity and directional sensitivities of the probes were obtained over a velocity range corresponding to the tunnel q between 5 and 10 in. H_2O and over the flow angles from -10^0 to $+10^0$. Details on the calibration procedures and complete information on data reduction methods are contained in Refs. 15 and 16.

Procedure to Establish Momentumless Conditions

A zero net momentum condition was desired for the injection and propeller-driven models. The traverse was placed at station $X/D=5$, so as to exclude the effects associated with the tail and to include a definitive excess region in the velocity profile, and the pitot-static probe was aligned along the axis of the body. In the case of Model 2, dynamic pressure scans were taken for a range of injection pressures suggested by preliminary testing. Application of a cylindrical control volume analysis, where the momentum flux past any transverse section of the wake (constant for all stations) is equated to that of the oncoming freestream, yields an expression for the drag of an axisymmetric body. The mean-flow data were integrated to determine the value of injection pressure necessary to satisfy $D \approx 0$. This calculation neglects the contributions from the viscous stresses (higher order terms) and turbulence (negligibly small in comparison to mean flow) that normally appear in the longitudinal Reynolds equation. For each injection pressure the drag values for horizontal and vertical scans were averaged.

In the case of Model 3, pressure traverses were taken for a range of rpm values of the propeller. Again the momentum balance was used in an iterative experimental procedure to find the momentumless operating condition.

Experimental Results

Wind Tunnel Flow

Since the wind tunnel used here has flexible vertical walls, the walls required fine adjustment before testing. After these adjustments were made, the flow angularity in the vertical and lateral planes was less than 1^0. For these experiments the flow was essentially uniform across the test section, a maximum 2% deviation from the centerline value, without the model. The axial pressure gradient was found to be essentially zero for the major part of the working test section. In addition, extensive checks on the symmetry of the profiles of all models tested with respect to peripheral angle were made. The maximum variations in dynamic pressure in the lower two quadrants opposite the strut where the primary measurements were made were less than $\pm 2\%$. The lower quadrants were selected for wake measurements in order to minimize the influence of the strut on the wake properties measured.

Drag Body Model (Model 1)

Model 1, a drag body, was studied primarily to provide a reference comparison case for the self-propelled bodies. Using Eq. (1) of Ref. 10, which includes the contribution of turbulent fluctuations, the average drag coefficient C_D was calculated to be 0.092. The variation of C_D with axial position showed a maximum deviation of 15%.

Mean velocity distributions for stations $X/D=2$, 5, 10, 20, and 40 at the nominal freestream dynamic pressure of 9.5 in. of H_2O are provided in nondimensional form in Fig. 3. They represent typical elementary shear flow profiles, where the velocity deficit spreads outward and decreases on the centerline as the flow proceeds downstream. Self-similarity of these mean-flow profiles was indicated, even for $X/D=2$ (see Ref. 15). All the mean-flow and turbulence data presented in this paper are normalized by the freestream velocity outside of the wake at the corresponding station, U_e. By using the values of U_e established for each X/D, the problem of small axial variation of U_e could be largely dispensed with.

Chevray's data[10] for fluid motion about a 6 to 1 oblate spheriod with a $Re_D=4.58\times10^5$, as compared to 6.18×10^5 for this model, reveal a greater rate of decay of the velocity deficit, while the data from Ref. 11 for a slender, axisymmetric body and $Re_D=0.49\times10^5$ agree extremely well with the present measurements.

The axial turbulence intensity profiles are shown in Fig. 4. These and subsequent turbulence intensity data were corrected for background turbulence by subtracting the value of the freestream turbulence intensity at the corresponding station. Such procedure is based on the assumption that the turbulence intensities inherent to different sources are statistically independent and are subject to linear superposition.

The axial turbulence profiles shown in Fig. 4 indicate that the peak value increases over a distance ranging from $X/D=2$ behind the body tail to $X/D=10$ and then decreases as it moves further downstream. The other two directional turbulence intensities exhibit similar trends. The major reason for this behavior lies in the convergence of wake near the body tail. By comparing the data, it was seen that the longitudinal turbulence intensities were higher than those in the other two directions. The radial shear stress profiles are given in Fig. 5.

Now, these results can also be compared with those obtained by Chevray and Bukreev et al. It was found[16] that the results in terms of turbulence intensities and radial shear stress were close to each other in magnitude.

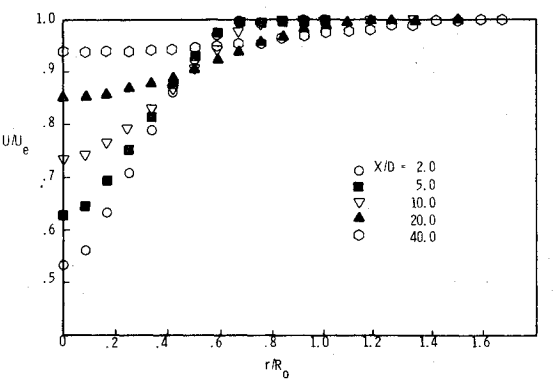

Fig. 3 Mean, axial velocity profiles for the drag-body model (Model 1).

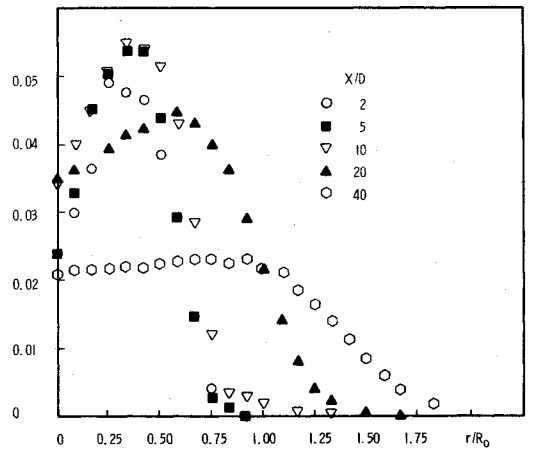

Fig. 4 Axial turbulence intensity profiles for the drag-body model (Model 1).

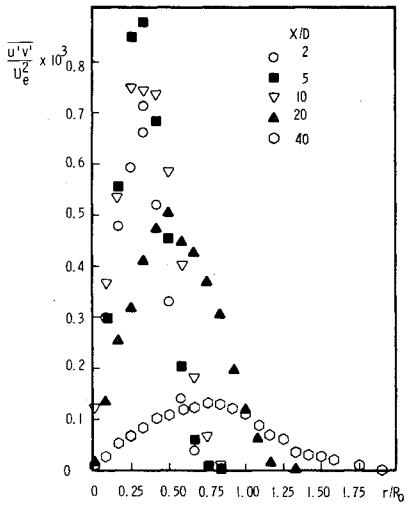

Fig. 5 Reynolds stress profiles for the drag-body model (Model 1).

Jet-Propelled Body (Model 2)

The estimated jet velocity required to produce a zero change of momentum flux for Model 2 was $1.14U_e$. This value reflects the nature of the experimental set-up used. In particular, if the jet had a different diameter or the body was shaped differently, a different jet efflux velocity would be necessary to achieve the momentumless state,i.e., a value of $U_j=3.64U_e$ was necessary for the disk experiments of Ref. 1. The degree to which this condition was realized in the wake flow of Model 2 is exhibited in the axial change of C_D. This showed a maximum C_D for $X/D=5$ to 40 of 1.7% of the total drag coefficient of the body. At $X/D=2$ the C_D was largest, and there was a 5.3% deficit in thrust required. This was attributed to the close proximity in which measurements were taken and the initial lower temperature of the jet, as compared to the freestream value.

Mean flow velocity profiles are shown in Fig. 6. These distributions are based on the average values obtained in the horizontal and vertical pressure scans since the operating injection pressure was defined that way due to the slight asymmetry in the injected flow and its corresponding effect on the total asymmetry of the wake flow. Because of the presence of the center body in the injection region, there is a velocity defect in the immediate vicinity of the centerline at stations $X/D=2$ and 5. Beyond the initial wake region, the velocity profiles resemble those of a combined jet and wake flow, if there were no center body. That is, there is a velocity excess region in the inner portion of the wake and a velocity deficit region in the outer part.

The axial turbulence intensity profiles are plotted in Fig. 7.

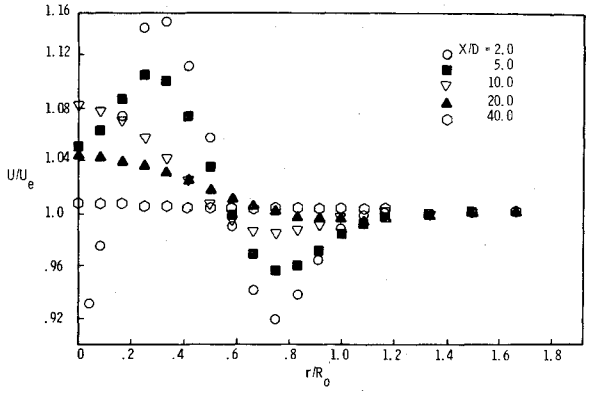

Fig. 6 Mean, axial velocity profiles for the jet-propelled model (Model 2).

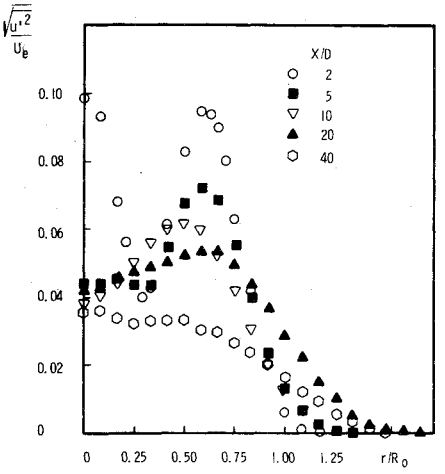

Fig. 7 Axial turbulence intensity profiles for the jet-propelled model (Model 2).

As expected, the profiles are very different from those for the streamlined body both in their distributions and their magnitudes. The profiles have some peculiar phenomena near the center of the wake and there are dips near $r/R=0.25$ at the stations close to the tail. These dips correspond to the radial locations where the downstream moving jet attains its maximum local velocity (cf. Figs. 6 and 7). The outer peaks can be clearly associated with the outer shear layer, which is formed between the jet and the surrounding wake produced by the cylindrical, external body. Convergence of this layer, induced by the geometry of the stern body, can be noticed between the stations $X/D=2$ and $X/D=10$. The radial and tangential turbulence intensity profiles display also significant variation in the inner portion of the wake.[16] The radial shear stress profiles (Fig. 8) show a dip and then a big peak (for $X/D=2$ and 5), which coincide with the local maxima of the shear values to be expected inside the inner and outer shear layers formed at the "sides" of the jet stream exhausted from the model. The inner shear layer forms between the jet and the wake of the stern; the outer layer is the same as previously mentioned. Note that in the outer portion of the model wake the sign of the shear stress is opposite to that of the streamlined body.

Since there are no published experimental data on a slender, streamlined body with a momentumless wake by injection available, the work used for comparison here is a study of a circular disk with air injection, which is neither slender nor streamlined.[1] The peak turbulence intensity and Reynolds stress for Model 2 are lower than Naudascher's data. The longitudinal turbulence intensities are higher than the radial and tangential ones, but the peak radial and tangential turbulence intensities measured here are close to the peak axial turbulence intensities by Naudascher. The decay rates of the turbulence intensity of Model 2 are much slower than in

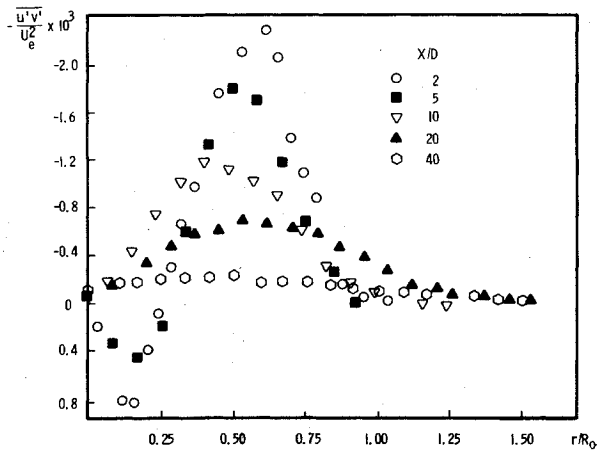

Fig. 8 Reynolds stress profiles for the jet-propelled model (Model 2).

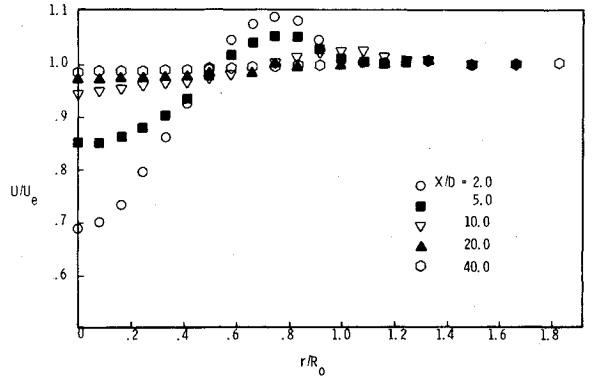

Fig. 9 Mean, axial velocity profiles for the propeller-driven model (Model 3).

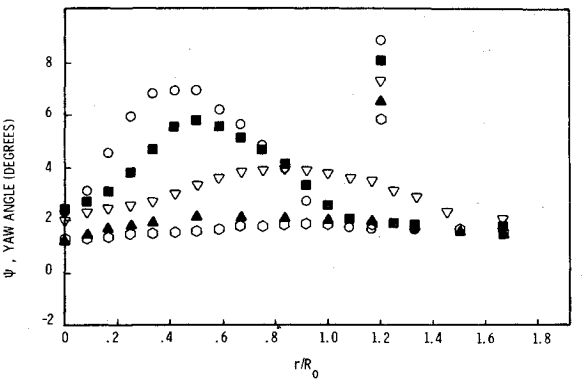

Fig. 10 Yaw angle (in degrees) profiles for the propeller-driven model (Model 3).

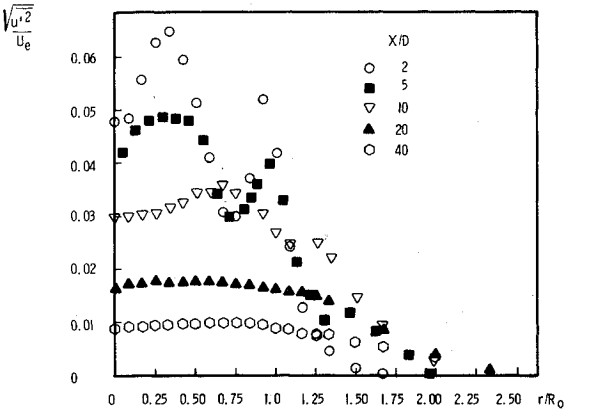

Fig. 11 Axial turbulence intensity profiles for the propeller-driven model (Model 3).

Naudascher's experiments. It was noted that the dip is higher than the peak in the Reynolds stress profiles for this model but the reverse is true for Naudascher's model.

Propeller-Driven Body (Model 3)

The degree of the momentumless condition for the propeller-driven model was examined as a function of X/D. For positions $X/D=5$ and 10, there was an excess thrust of less than 2.4%, while stations $X/D=20$ and 40 showed a slight drag with a maximum C_D of less than 3.5% of the actual C_D of the body. The measurements at $X/D=2$ indicated an excess thrust of about 20%, but there were significant measurement problems at this station due to the large velocity gradients and high turbulence level. Overall, these results are judged to show an essentially self-propelled condition.

Nondimensional axial velocity profiles for the five stations mentioned previously are given for the propeller-driven model in Fig. 9. The basic character of momentumless wake is exhibited in these velocity variations, i.e., a velocity defect region and a velocity excess region. However, the velocity excess region is in the outer part of the shear flow, which is contrary to the jet-propelled case.

The flow angularity in the yaw direction produced by the propeller is indicated in Fig. 10. These measurements show that there was a maximum deviation of 5.26^0 from the freestream flow. The swirl velocity distributions were determined from these angles. Since the undisturbed flow angularity was not zero, a maximum of -0.78^0, the curves did not pass exactly through zero at $r=0$ in. The profiles display a solid body of rotation behavior ($v_t \sim r$) in the inner region and decay to approximately zero in the outer region.

On a log-log graph, the axial centerline velocity deficit decay was found to be linear with a decay rate of $(X/D)^{-0.969}$. Although the major part of the momentum transferred by the propeller to the fluid was in the outer portion of the wake for this model, the downstream rate of decrease of $|(U_e-U)_{max}/U_e|$ compares favorably with data from Ref. 14, where the momentum transfer was confined primarily to the center wake region. The difference is attributed to the higher pitch of the present propeller and its extension beyond the boundary layer of the body. A comparison of the decay rate for this model with that of Model 1 shows that the initial decay is faster for the propeller-driven body than the drag body. However, the rates of decay are essentially the same beyond $X/D=10$.

The turbulence intensity profiles in the longitudinal direction are plotted in Fig. 11. The radius of the wake is much wider than that for the other two models, and the longitudinal turbulence intensity profiles have more than one peak at stations $X/D=2$, 5, and 10. The second peak (around $r/R=1$) corresponds with the tips of the propeller blades. Another significant point to be noticed is that the turbulence intensity profiles are quite flat and widely spread after $X/D=10$.

The Reynolds stress profiles (Fig. 12) in the radial direction each have a peak and then a dip at stations near the body. The peak corresponds to the local maximum value of shear stresses inside the shear layer formed near the hub of the propeller, and the dip is related to the helical shear vortices generated by the tips of the propeller blades. There is no initial convergence in the radial direction of the shear layer, opposite to that observed for the second model, because there was no extended tail body downstream of the propeller. The magnitudes of the Reynolds shear stresses decay very rapidly downstream after the station $X/D=10$ and the profiles become very flat. Reynolds stress values in the tangential direction were bigger than for the other two models. We observed an even higher tangential shear stress than that in the radial direction at the stations near the tail of the body. This is due to the presence of swirling in the flowfield due to the propeller.

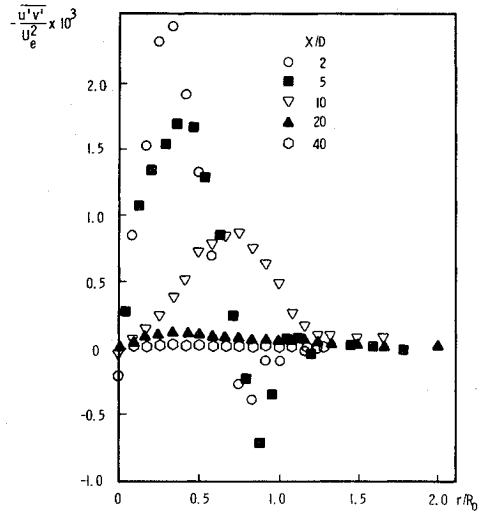

Fig. 12 Reynolds stress profiles for the propeller-driven model (Model 3).

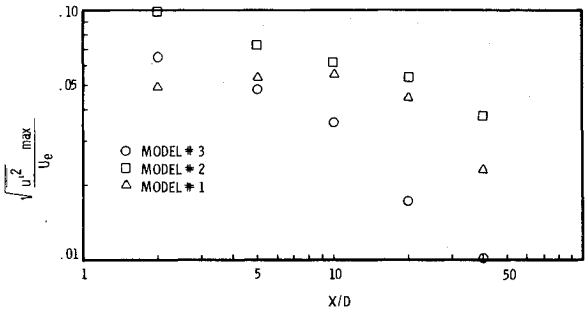

Fig. 13 X/D decay for maximum axial turbulence intensity for all three models.

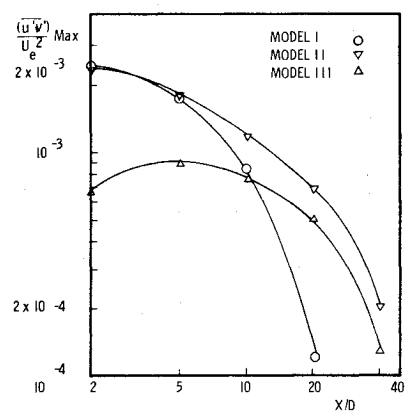

Fig. 14 Comparison of maximum stress decay for all three models.

Figures 13 and 14 compare the decay rates of peak turbulence intensity and Reynolds stress for this model (Model 3) with the corresponding values for the other two models. In general, the decay rates for this model are much higher except for the initial distance behind the body ($X/D<5$), where the decay rates for Model 2 and Model 3 are comparable. The longitudinal turbulence intensities for Model 3 are lower than those in the other two directions for this model, while for the other two models the longitudinal turbulence intensity is higher than that in the other two directions[16]. It can be concluded that all the turbulence characteristics of the wake of Model 3 are very different from the wake turbulence characteristics of Models 1 and 2 both in magnitude and profile distributions of turbulence intensity and shear stress.

The turbulence data for Model 3 have been compared with the results obtained by Gran.[14] The peak radial shear stresses

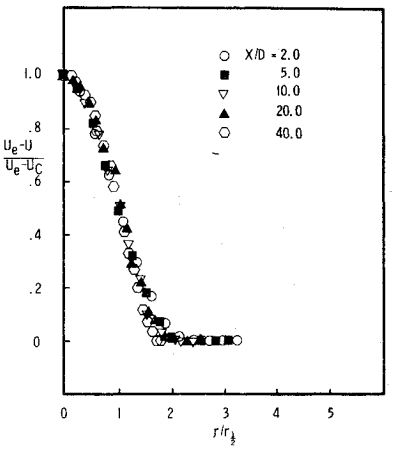

Fig. 15 Similarity plot of mean velocity profiles for the drag body (Model 1).

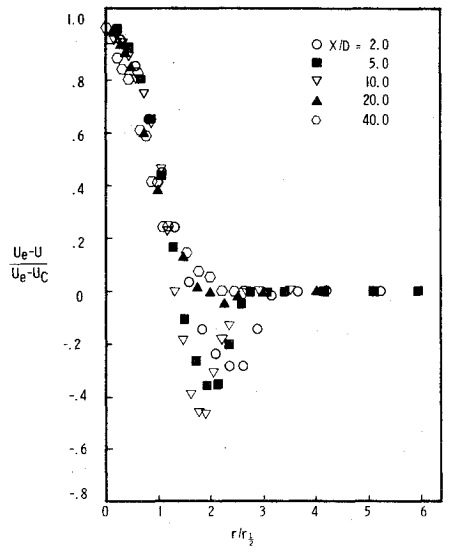

Fig. 16 Similarity plot of mean velocity profiles for the propeller-driven body (Model 3).

for the two models are similar, but the axial turbulence intensity for Gran's model is higher than that for Model 3, although the decay rates are similar. The differences shown might be caused by the different characteristics and performance of the propellers. No performance data on Gran's propeller is available.

A question usually asked when studying wakes is the problem of self-similarity of the wake properties. Figures 15 and 16 show examples of similarity profiles for the Models 1 and 3. It can be recognized that except for the mean velocity behind the drag model (Model 1), the self-similarity condition is not yet fully attained even at $X/D=40$. However, the outside portion of the wake appears to be close to the self-preservation condition at $X/D>5$.

Momentum and Energy Balance Analyses

To obtain an insight into the mechanisms of momentum and energy transformation and to assess the reliability of the experimental data, momentum and energy balance analyses were made. A useful form of the momentum equation is derived by integrating the first equation of Reynolds over a cylindrical control surface and neglecting the viscous stress under the assumption of high Reynolds numbers. The resulting momentum equation for the axial direction[17] can be reduced to

$$-\frac{C_D}{2}=2\int\left[\frac{U_d}{U_e}\right]^2\frac{r}{R}\,d\frac{r}{R}-2\int\frac{U_d}{U_e}\,\frac{r}{R}\,d\frac{r}{R}$$

$$+\int \frac{\overline{P_A}}{P_0}\,\frac{r}{R}\,d\,\frac{r}{R}+\int \frac{\overline{u'^2}}{U_e^2}\,\frac{r}{R}\,d\,\frac{r}{R}$$

where $U_d = U_e - u$. The first two terms on the right-hand side represent the net change in mean momentum flux over the control surface, the third term represents the effect of the pressure difference between the final and initial sections, and the last term accounts for the difference in turbulent momentum flux. The values of the integrals were calculated for the three models and for each X/D station, and are discussed in some detail in Ref. 16. In brief summary, it was found that all the values of momentum integrals changed significantly near the tail of the three bodies and then, more downstream, tended to stabilize or reduce gradually.

The turbulence and pressure terms were of non-negligible magnitude and they may have to be evaluated if an exact zero-momentum condition is desired. This may be important for the stations where the turbulence intensity is high (near wake of Model 2) and static pressure variations are large (Model 3). In general, however, the drag coefficients for Model 2 and Model 3 were fairly close to zero and the results obtained were judged as very reasonable.

The energy equation for a steady, axisymmetric flow of an incompressible fluid without a spiral component and under the assumption of a Reynolds number sufficiently high so that the work done by viscous stresses is negligible becomes[17]

$$2\int\left[\frac{u}{U_e}\left(\frac{u^2+v_r^2}{U_e^2}\right)-1\right]\frac{r}{R}\,d\,\frac{r}{R}$$

$$+2\int\frac{u}{U_e}\,\frac{\overline{P_A}}{P_0}\,\frac{r}{R}\,d\,\frac{r}{R}$$

$$+4\int\left(\frac{u}{U_e}\,\frac{\overline{u'^2}}{U_e^2}+\frac{v_r}{U_e}\,\frac{\overline{u'v'}}{U_e^2}\right)\frac{r}{R}\,d\,\frac{r}{R}$$

$$+2\int\left(1-\frac{u}{U_e}\right)\frac{r}{R}\,d\,\frac{r}{R}$$

$$+4\int\int\left[\frac{\overline{u'v'}}{U_e^2}\left(\frac{\partial u/U_e}{\partial r/R}+\frac{\partial v_r/U_e}{\partial x/R}\right)\right.$$

$$\left.+\frac{\overline{u'^2}}{U_e^2}\,\frac{\partial u/U_e}{\partial x/R}+\frac{\overline{v'^2}}{U_e^2}\,\frac{\partial v_r/U_e}{\partial r/R}\right.$$

$$\left.+\frac{\overline{w'^2}}{U_e^2}\,\frac{v_r/U_e}{r/R}\right]d\,\frac{r}{R}\,d\,\frac{x}{R}=0$$

The first and fourth terms come from the energy equation of mean motion. The second, third, and fifth terms represent the energy contributions due to pressure differences, turbulence, and shear stresses, respectively. Since the radial velocity was not obtained from the measurements, some rough estimates were made via the continuity equation. The values of energy integrals were calculated for all the cases considered (three models at five axial stations; see Ref. 16 for details) and the deviation of the sum of the integrals from zero, Δ, was obtained. The results of these calculations show that the deviation Δ is very small for Models 2 and 3; Δ is somewhat larger, but still small, for Model 1. The pressure and turbulence contributions for Models 2 and 3 are generally larger than those for Model 1. Although the analysis cannot serve as a truly sensitive detection of the accuracy of turbulence measurements, the degree to which the energy equations are satisfied suggests that the results presented are reliable and of good quality.

Conclusions

After comparing the present results for the three models with each other and with experimental results by others, some general conclusions may be drawn. First, the flowfields behind the tested bodies are quite different from one another. The wake of Model 1 is narrower than that of Model 2, which in turn is narrower than that of Model 3. The axial turbulence intensity profiles are smooth curves with a single peak for Model 1, while the corresponding curves for Models 2 and 3 display double peaks, at least at stations $X/D<20$. All these peaks disappear far downstream, and the rate of decay for Model 3 is the fastest among the three models. The magnitude of the axial turbulence intensity in the wake of Model 1 is relatively lower than that for Model 3, which is lower than that for Model 2. The radial shear stress profiles are smooth curves with a single peak for Model 1 and curves with a peak and a dip for Models 2 and 3. The presence of two extreme values of radial shear stress (corresponding to the peak and the dip) for these models is related to the presence of two shear layers, inner and outer, formed between the propelling air stream and the inner or outer wake. The highest values of the axial turbulence intensity and the radial shear stress were observed in Model 2. The decay rates of these quantities were fastest for Model 3, and, consequently, the magnitude of these quantities for Model 3 were even lower than for the drag body (Model 1) at farther stations ($X/D=20$ and 40). The tangential shear stress profiles showed a high peak and a big dip for Model 3. The magnitude of the tangential shear stress was relatively low for Models 1 and 2 as compared to Model 3, which exhibits the highest value at near stations but also has the highest rate of decay.

Second, for the cases presented here, the Momentum Balance analysis shows that, in general, the result obtained for Models 2 and 3 correspond to the desired zero-momentum case. The Energy Balance analysis suggests that the results presented are of good quality, in general, but the analysis cannot serve as a truly sensitive detection of the accuracy of turbulence measurements. Nevertheless, such an analysis gives an insight into the overall flow structure and the mechanism of energy transformation.

Last, the wake development of a blunt-body (disk) driven by a high speed central jet to yield a zero-momentum wake as studied by Naudascher[1] is significantly different from the momentumless wake development of a slender, streamlined body driven by a peripheral jet or propeller.

References

[1] Naudascher, E., "Flow in the Wake of Self-Propelled Bodies and Related Sources of Turbulence," *Journal of Fluid Mechanics*, Vol. 22, Pt. 4, 1965, pp. 625-656.

[2] Hall, A. A. and Hislop, G. S., "Velocity and Temperature Distributions in the Turbulent Wake Behind a Heated Body of Revolution," *Proceedings of the Cambrdige Philosophical Society*, Vol. 34, 1938, p. 345.

[3] Cooper, R. D. and Lutzky, M., "Exploratory Investigation of the Turbulent Wakes Behind Bluff Bodies," DTMB R&D Rept. No. 953, Oct. 1955, David Taylor Model Basin, Washington, D.C.

[4] Ilizarova, L. I. and Pochkina, K. A., "Experimental Study of a Wake Behind a Body of Revolution," *Prom. Aerodynamika*, No. 23, 1962.

[5] Ridjanovic, M., "Wake with Zero Change of Momentum Flux," Ph.D. dissertation, 1963, University of Iowa, Iowa City, Iowa.

[6] Carmody, T. "Establishment of the Wake Behind a Disk," *ASME Transactions: Journal of Basic Engineering*, Vol. 87, Dec. 1964, pp. 869-882.

[7] Wang, H., "Flow Behind a Point Source of Turbulence," Ph.D. dissertation, 1963, University of Iowa, Iowa City, Iowa.

[8] Ginevskii, A. S., Pochkina, K. A., and Ukhanova, L. N., "Propagation of Turbulent Jet Flow with Zero Excess Momentum," *Fluid Dynamics Academy of Sciences USSR*, Vol. 1, Nov.,-Dec. 1966, Faraday Press, Ind.

[9] Buckinskaya, E. K. and Pochkina, K. A., "Investigation of Vortex Wake Behind a Body of Revolution," *Prom. Aerodynamika*, No. 23, 1962.

[10] Chevray, R., "The Turbulent Wake of a Body of Revolution," *ASME Transactions: Journal of Basic Engineering*, Vol. 90, Dec. 1968, pp. 275-284.

[11] Bukreev, V. I., Kostomakka, V. A., and Lytkin, Y., "Axisymmetric Turbulent Wake Behind a Streamlined Body," *Siberskaw, Otdelinie An SSSR, Instituk Gidrodinamiki, Dinamika Sploshhoi Sredy*, No. 10, 1972, pp. 202-207.

[12] Hokenson, G. J. and Schetz, J. A., "Free Turbulent Mixing in Axial Pressure Gradients," *ASME Transactions: Journal of Applied Mechanics*, Vol. 95, June 1973, pp.375-379.

[13] Bukreev, V. J., Kostomakha, V. A., and Lytkin, Yu, M., "Turbulent Energy Balance in Axisymmetric Wakes Behind Differently Shaped Bodies," *Prikladnaya Mikhanika i Tekhmicheskaya Fizeka*, No. 1, 1974, pp. 165-168.

[14] Gran, R. L., "An Experiment on the Wake of a Slender Propeller-Driven Body," Rep. for ONR, June 1973, TRW Systems, Los Angeles, Calif.

[15] Swanson, R. C., Jr., Schetz, J. A., and Jakubowski, A. K., "Turbulent Wake Behind Slender Bodies, Including Self-Propelled Configurations," VPI Aero-024, Sept. 1974, VPI & Su, Blacksburg, Va. available through NTIS.

[16] Chieng, C. C., Jakubowski, A. K., and Schetz, J. A., "Investigation of the Turbulent Properties of the Wake Behind Self-Propelled, Axisymmetric Bodies," VPI-Aero-025, Sept. 1974, available through NTIS.

[17] Rouse, H., "Distribution of Energy in Regions of Separations," *La Houille Blanche*, Vol. 3, May 1960.